Journal of the Korean Physical Society, Vol. 74, No. 7, April 2019, pp. 660∼673

Quantitative Investigation into the Relation between Force Chains and Stress Transmission During High-Velocity Compaction of Powder

Wei Zhang, Jian Zhou, Xue-Jie Zhang and Kun Liu*
Institute of Tribology, Hefei University of Technology, Hefei 230009, China

(Received 26 October 2018, in final form 1 December 2018)

High-velocity compaction (HVC), an innovative approach to obtain green compacts with high and uniform density, is widely used in the powder metallurgy industry. In this study, meso force chains, macro stress transmission, and their relation were investigated using the discrete element method. The simulation details of HVC and the quantitative characterization of force chains and stress transmission were shown. Then, the relation between force chains and stress was investigated. The evolution of force chains showed the same change tendency as the stress distribution. They evolved from top to bottom and then reflected backwards in HVC while they did not show this trend in conventional compaction. The strength of the force chains maintained good consistency with the stress magnitude. Meanwhile, the length of the force chains presented a negative correlation with the stress magnitude, and high stress may cause new force chains to shorten. The average collimation coefficient was affected by the transmission of stress, and the short force chains had better straightness. Furthermore, force chains parallel to the direction of gravity were observed in the region with no stress concentration. The directional coefficient of force chains also had the same fluctuation trend as the variation in the principal stress angle.

PACS numbers: 45.70.Mg, 45.70.−n
Keywords: High-velocity compaction, Granular matter, Stress, Force chains
DOI: 10.3938/jkps.74.660

I. INTRODUCTION

High-velocity compaction (HVC) is a novel forming method in the powder metallurgy industry. The essential principle of HVC is to accomplish the densification of a powder rapidly by applying a high impact load instantaneously. Compared to conventional compaction (CC), HVC almost has the same steps as uniaxial die-pressing, but the key difference is that HVC can be 500–1000 times faster than CC. The powder is compacted by an impact object traveling at a speed of 2–30 m/s, and in HVC densification is accomplished in less than 20 ms. While CC applies a load slowly by controlling the pressure or travel and finishes compressing in seconds [1]. During HVC, the powder undergoes quicker processes of reorganization, rearrangement, and densification relative to CC. Hence, HVC can achieve higher density and better density homogenization than CC. Experimental studies have been widely carried out to investigate the green density, spring back, Vickers hardness, bending strength, tensile strength, and characteristics of the stress wave during HVC [1–5]. The experimental method can present the real condition of HVC, but it can only capture its macro details. Numerical simulation methods, such as the finite element method (FEM) [6,7] and the multi-particle FEM (MPFEM) [8,9], have been used to investigate the macro and the micro scale characteristics of powders. But FEM disregards the interaction between particles, and the MPFEM can only simulate a small amount of powder that is far less than that in reality because limits on the calculation costs. Powder, which is essentially granular matter, can be considered a discrete flowing medium in forming dies. Hence, the discrete element method (DEM) is a feasible method to study HVC and has been used to investigate the rapid motion and temperature distribution of the powder in HVC [10,11]. The DEM can also be used to examine the dynamic evolution of the mechanics of the powder on different scales (micro, meso and macro scales) in HVC.

At the meso scale, force chains are quasi-linear structures of adjacent particles that squeeze one another under gravity or an external load. They can play an important role in promoting the motion of the powder and forming its stable skeleton. Meanwhile, the quantitative characteristics of force chains in HVC may present more dramatic and dynamic changes than those in CC. These characteristics are helpful in understanding the evolutions of the local structure and the motion of the powder in HVC. At the macro scale, the local stress distribution of the powder in HVC is also significant for densification

*E-mail: liukun@hfut.edu.cn

and is different from CC because the impact load in HVC may cause the stress to be transmitted sequentially [4, 12,13]. Hence, an accurate description of the stress distribution on a macro scale in HVC is necessary. As we mentioned previously, the force chains and the stress in HVC are all vital for further study and helpful for illustrating the mechanism of powder densification.

More importantly, the crucial problem about the multi-scale mechanism of powder compaction involves linking the force chains and the stress from different scales. However, some researchers [14, 15] only change the stress to observe the corresponding alteration of force chains. Different pressure levels have been applied to the system. They point out that the increasing external stress can make force chains denser and stronger and that the force chain communities can be sensitive to external stress. Others investigate the relation between macro stress and the buckling of force chains [16,17] and the relation between shear stress and force chain formation [18, 19]. They point out that the peak stress ratio is related to the number of buckling force chains and that shear strain localization can cause force chains to be sparse in the shear band. Limitations exists in the explanation of the interconnection between stress and force chains, and the quantitative correspondence is not reflected well. An external stress causes an inner stress response of the powder and the inner stress can be related to the evolution of meso-scale force chains. The stress may cause the force chains to evolve, and the force chains may provide transfer paths of stress. The relationship between force chains and stress is also beneficial for examining densification from the macro scale to the micro scale in HVC. Thus, depicting the mutual action mechanism of stress and force chains in HVC is essential.

In the current work, DEM simulations are employed to study the evolution of force chains and stress in HVC. Firstly, the details of the modeling are provided, and the analysis methods of force chains and stress are shown. The evolution of force chains and the distribution of stress in HVC are compared to those in CC. Secondly, the quantitative characteristics of force chains (such as length, strength, directional coefficient, and collimation coefficient [including their distribution]) and the distribution and the direction of the stress in HVC are investigated to link the force chains and stress at the meso and the macro scales, as well as to investigate their relation. Meanwhile, the mutual influence of stress and force chains is discussed.

II. METHODOLOGY

1. DEM modeling

In this research, we use the DEM to simulate HVC. The key motion formulations in the DEM to describe the motion of one particle involve Newton's second law of motion:

$$\begin{cases} m_p\mathbf{g} + \sum \mathbf{f}_i = m_p \dfrac{\mathrm{d}\mathbf{v}_p}{\mathrm{d}t} \\ \sum \mathbf{f}_i \mathbf{r}_i = I_p \dfrac{\mathrm{d}\omega_p}{\mathrm{d}t}, \end{cases} \tag{1}$$

where m_p, $\mathbf{v}_p$ and ω_p are the mass, translational velocity, and angular velocity of particle p, respectively. $\mathbf{f}_i$ and $\mathbf{r}_i$ are the contact force and the position vector from contact to particle of the i-th contact, respectively.

The displacement, velocity, and acceleration of every particle can be calculated by using Newton's second law of motion. The contact force is an important part of describing the interaction of particles. The Hertz-Mindlin contact model [20] is used to calculate the contact force between two particles, but that model can only describe the elastic deformation of particles. However, the powder in HVC can undergo plastic deformation. If the overlap of two particles is greater than the threshold, then the displacement softening model [20] is added to the Hertz-Mindlin contact model, and the resulting scheme can describe the plastic deformation of particles. Any adhesive effects are neglected in the analysis. The elastic-plastic work can be reflected by the overlap of particles, and the frictional work can be reflected by Coulomb's law of friction in the tangential contact model. The viscous damping has also been considered in the energy dissipation. The normal contact force is determined as follows [10,21]:

$$F^e_{nij} = \frac{4}{3}\tilde{E}\sqrt{\tilde{R}}\alpha^{\frac{3}{2}} - \eta_n\bar{v} \quad \text{(elastic region)}, \tag{2}$$

$$\sigma = 3\sigma_0, \tag{3}$$

$$a = c\sqrt{2\alpha\tilde{R}}, \tag{4}$$

$$F^{\mathrm{p}}_{nij} = 2\sigma{<}d{>}a - \eta_n\bar{v} \quad \text{(plastic region)}, \tag{5}$$

where σ is the equivalent stress, σ_0 is the yield stress, α is the overlap between two particles, η_n is viscous normal damping coefficient, and $\bar{v}$ is the relative velocity between two particles. a is the contact radius, $\tilde{R}$ and $\tilde{E}$ are the equivalent radius and elastic modulus, respectively, and $<d>$ is the average diameter. The material invariant is $c^2 = 1.43$ for ideally plastic material behavior, and $\tilde{R} = \frac{R_1R_2}{R_1+R_2}$ and $\tilde{E} = \left(\frac{1-v_1^2}{E_1} + \frac{1-v_2^2}{E_2}\right)^{-1}$, with subscripts "1" and "2" meaning two particles in contact labelled 1 and 2. Equation (2) depends on the Hertz contact model. Equation (3) depends on the von Mises yield criterion. By combining Eq. (2), Eq. (3), Eq. (4) and Eq. (5), we can calculate the threshold of overlap as

$$\alpha_{\max} = \frac{9\sqrt{2}c{<}d{>}\sigma_0}{2\tilde{E}}. \tag{6}$$

The tangential contact force is determined as follows [10,

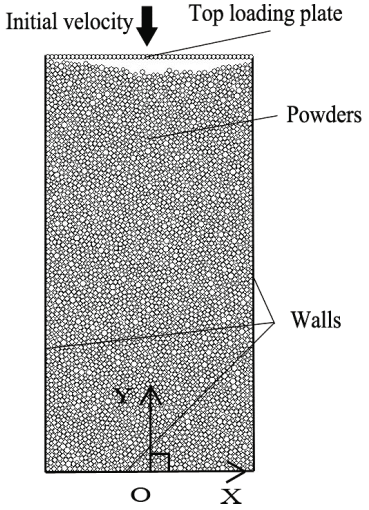

Fig. 1. DEM model of HVC.

21]:

$$F_{tij} = \lambda u_t F_{nij}^{1/3} \left(\frac{2\left(6\tilde{R}(1-\nu)\tilde{G}^2\right)^{1/3}}{2-\nu} \right) + \mu F_{nij}(1-\lambda) - \eta_t \bar{v}_s, \tag{7}$$

where u_t and $\bar{v}_s$ are the relative displacement and the relative slip velocity between two particles, η_t is the viscous tangential damping coefficient, μ is the friction coefficient, $\tilde{G}$ is the equivalent shear modulus and $\tilde{G} = \frac{1}{2}(G_1 + G_2)$. If $F_{tij} < \mu F_{nij}$, $\lambda = 1$. If not, $\lambda = 0$. Equation (7) depends on the Mindlin contact model and Coulomb's law of friction.

The normal and the shear stiffnesses in compression for the displacement softening model can be calculated as follows [22]:

$$\begin{cases} K_c^n = \dfrac{E}{\sqrt{3}(1-v)}, \\ K_c^s = \dfrac{E(1-3v)}{\sqrt{3}(1-v^2)}. \end{cases} \tag{8}$$

The normal stiffness in tension is the same as the normal stiffness in compression. Other micro-parameters of the displacement softening model are the same as shown in Ref. [23].

Through the DEM, we establish the physical model of HVC. As shown in Fig. 1, the ferrous particles are surrounded by three fixed walls of the die and a top loading plate, which is composed of 50 particles with diameters of 200 μm. Although the ferrous powder is not perfectly round on reality, we suppose that they are disks to investigate the force chains and the stress more easily. Gravity is applied to the model. The width and the height of the model are $W = 10$ mm and $H = 20$ mm, respectively. The simulation details of the HVC are described below.

Table 1. Simulation parameters.

Name of parameter	Symbol	Value
Number of particles	N	4500
Particle density	ρ	7800 kg/m^3
Particle size	d	150 ∼ 270 μm
Normal contact stiffness (particle to wall)	k_n	1.E8 N/m
Tangential contact stiffness (particle to wall)	k_t	1.E8 N/m
Initial porosity	β_0	0.2
Viscous normal damping coefficient	η_n	0.079
Viscous tangential damping coefficient	η_t	0.079
Friction coefficient (particle to wall)	$\mu_{\text{p-w}}$	0.3
Friction coefficient (particle to particle)	$\mu_{\text{p-p}}$	0.3
Poisson's ratio	ν	0.25
Elastic modulus	E	209 GPa
Yield stress	σ_0	394 MPa
Impact height	h	0.25 m

We attribute the initial velocity $v_0 = 2.21$ m/s, which satisfies the condition of HVC (calculated by $v_o = \sqrt{2gh}$, impact height $h = 0.25$ m), along the y-direction and an equivalent mass of 50 kg to the top loading plate to simulate the loading progress of dynamic impacting. Then, we record the first position and other information about the particles. Subsequently, we iteratively calculate new information on the particles to satisfy the conditions of equilibrium of force. Finally, we finish the calculation when the kinetic energy of the system becomes zero and the relative error is less than 0.005%. Under this condition, the entire simulation time is 4.59 ms. Although the final overlaps between particles may be larger than 5% of the average radius, the overlap is reasonable in this simulation. Because non-linear contact model is used and the normal force in displacement softening model is not calculated directly from the overlap [20]. Martin *et al.* [24] also apply the elastic-plastic contact law to simulate powder compaction with a relative density larger than 90% based on the DEM. Moreover, we only analyze the first loading stage of the powder in HVC because the compact pressure dominants the first peak [4], and the loading stage has the most significant influence on the densification of the powder.

The initial porosity in this system is 0.2, which was calculated by using the ratio of the area deviation between the system and all particles (not including the area of overlap) to the area of system. We suppose that the particle size distribution is an uniform distribution [4] and is in the range of 150–270 μm, with an average diameter of 210 μm. For problems involving impact between particles, local damping is inappropriate [20], the coefficient of restitution (ε) is 0.78 [25], and the viscous normal damping coefficient can be calculated as follows [26]:

$$\eta_n = -\frac{\ln(\varepsilon)}{\sqrt{\ln^2(\varepsilon) + \pi^2}}. \tag{9}$$

The viscous tangential damping coefficient is the same as the viscous normal damping coefficient. A lower safety

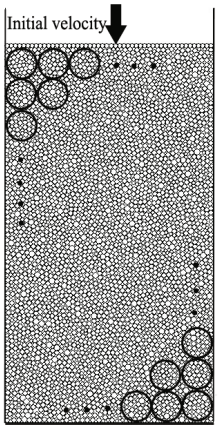

Fig. 2. Distribution of MCs.

factor of 0.25 on the time step is chose to ensure the solution precision during rapidly changing conditions [20]. Details of the simulation parameters are shown in Table 1.

2. Analysis method of stress distribution

Stress is a continuous medium tensor and exists at any position in the continuum. As stress in a discrete medium only occurs in a range of parts, it should be calculated by averaging the contact force at each particle of the selected parts. To ascertain stress transmission and capture the dynamic change of stress localization, we use the dynamic measurement circle (MC) [20] to calculate the stress in each part and to realize the distribution of stress. In each MC, we obtain the average stress tensor by averaging all the contact forces with the volumes and relative positions of the particles. The positions and the number of MCs can be changed with the progress of HVC to ensure that the powder system is filled with MCs with a radius of approximately eight times that of the average radius of powder (Fig. 2). Stress can be quantitatively described as [20]

$$\begin{aligned}\sigma_{ij} &= \frac{1-\beta}{\sum_{N_\mathrm{p}} V^\mathrm{p}} \sum_{N_\mathrm{p}} \sum_{N_\mathrm{c}} |\mathbf{x}^\mathrm{c} - \mathbf{x}^\mathrm{p}| \mathbf{n}^{\mathrm{c,p}} \mathbf{F}^\mathrm{c} \\ &= \frac{1}{V_\mathrm{MC}} \sum_{N_\mathrm{p}} \sum_{N_\mathrm{c}} |\mathbf{x}^\mathrm{c} - \mathbf{x}^\mathrm{p}| \mathbf{n}^{\mathrm{c,p}} \mathbf{F}^\mathrm{c},\end{aligned} \tag{10}$$

where β is the porosity in the MC; N_p and N_c are the number of particles in the MC and the number of contacts of each particle, respectively; V_p is the volume of the particle; V_MC is the volume of the measure circle; x_c and x_p are the positions of the contact and the particle, respectively; F^c is the contact force; and $n^{\mathrm{c,p}}$ is the unit normal vector from the contact to the particle, with subscripts i and j representing the x-direction and the y-direction, respectively.

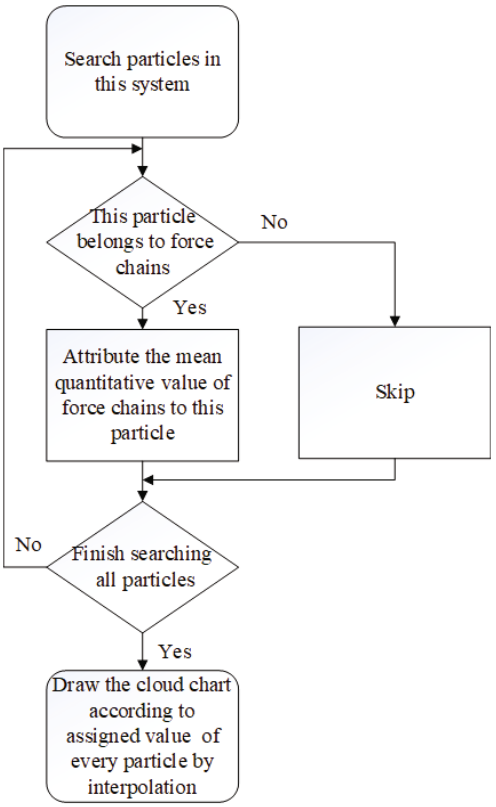

Fig. 3. Numerical calculation of the spatial distribution of force chain characteristics.

3. Quantitative analysis of force chains

Many methods, like minor principal stress method [27], can be used to identify force chains. To analyze the force chains more easily, we first define the force chain that satisfies the three conditions mentioned in Ref. [28], that is, (1) length condition: a force chain should include more than two particles; (2) magnitude of the contact force condition: the contact force that constitutes the force chains should be greater than the average contact force of the system; and (3) orientation of contact force condition: the adjacent contact pairs should have a sharp angle less than the threshold, which is 180° divided by the average coordination number. According to the above conditions, we extract information on the force chains from the DEM model at selected time steps. Noticeably, the algorithm for identifying force chains will search all particles from top to bottom according to their y-coordinates, and force chains that coincide with other longer force chains will be eliminated.

After acquiring the information on force chains in HVC, we use number, length l_i, strength p_i, directional coefficient σ_i, and collimation coefficient δ_i to describe the force chains quantitatively. Details of the force chain quantitative characteristics are presented in Eq. (10), Eq. (11) and Eq. (13). Moreover, we analyze the distribution of some force chain characteristics. First, we es-

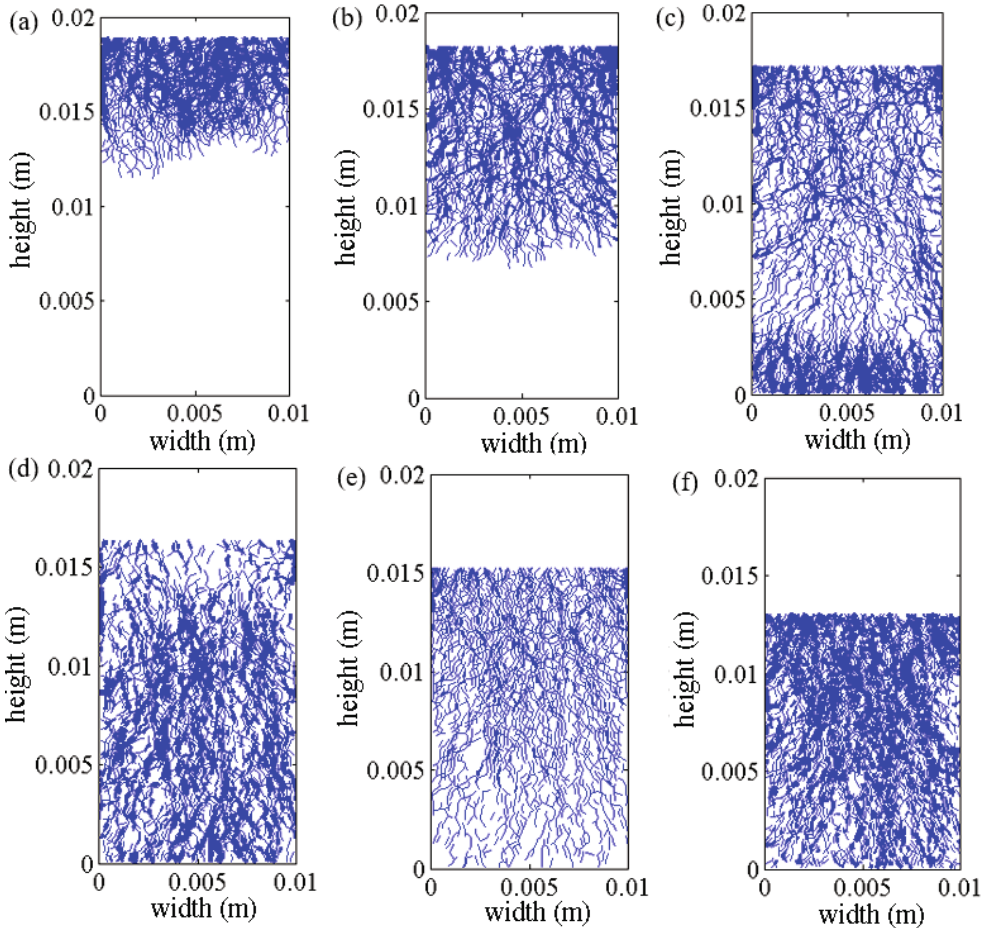

Fig. 4. (Color online) Structure of force chains at different moments (0.5, 0.8, 1.3, 1.7, 2.25, and 4 ms).

timate whether a particle belongs to force chains. Then, we attribute a quantitative value to the particle if it belongs to force chains. Finally, we search all particles in this system and draw the contour plots of the spatial distribution of the characteristics of force chains by using the interpolation method. Specifically, the quantitative characteristics are averaged if a particle belongs to more than one force chain. The detailed numerical calculation is shown in Fig. 3.

III. RESULTS AND DISCUSSION

1. Evolution of force chains and distribution of stress

Figure 4 shows the structure evolution of force chains at different moments. A thick line means great contact force. The structures of force chains can intersect as a network to provide load supporting capacity. The total simulation time is 4.59 ms, and it describes the first impact of the top loading plate. Accordingly, we choose particular moments (0.5, 0.8, 1.3, 1.7, 2.25, and 4 ms) that can clearly show how the force chains alter their structure and distribution, and the chosen moments are the same as there in Ref. [29]. First, at 0.5, 0.8, and 1.3 ms, the force chains seem to spread downward in this system. At the same time, the force chains with greater contact force evolve from top to bottom. Then, they concentrate in the middle part at 1.7 ms. Next, they converge at the top of this system at 2.25 ms. Finally, they gradually spread within the whole system at 4 ms. In general, we observe that positions of force chains with greater contact force change from top to bottom and then from bottom to top, ultimately becoming uniform gradually. Moreover, the relation between the spread velocity of force chains and the sound velocity in the particles may reveal the link between dynamic characteristics at the meso scale and at the macro scale. Every force chain is composed of particles with different velocities and will be able to break or reorganize in different moments, so the spread velocity of force chains is difficult to define and capture. The force chains' velocity may be calculated from the differences between the positions of the force chains in a very short time, but the algorithm would be complex. Another interesting topic would be to capture and characterize the force chains'

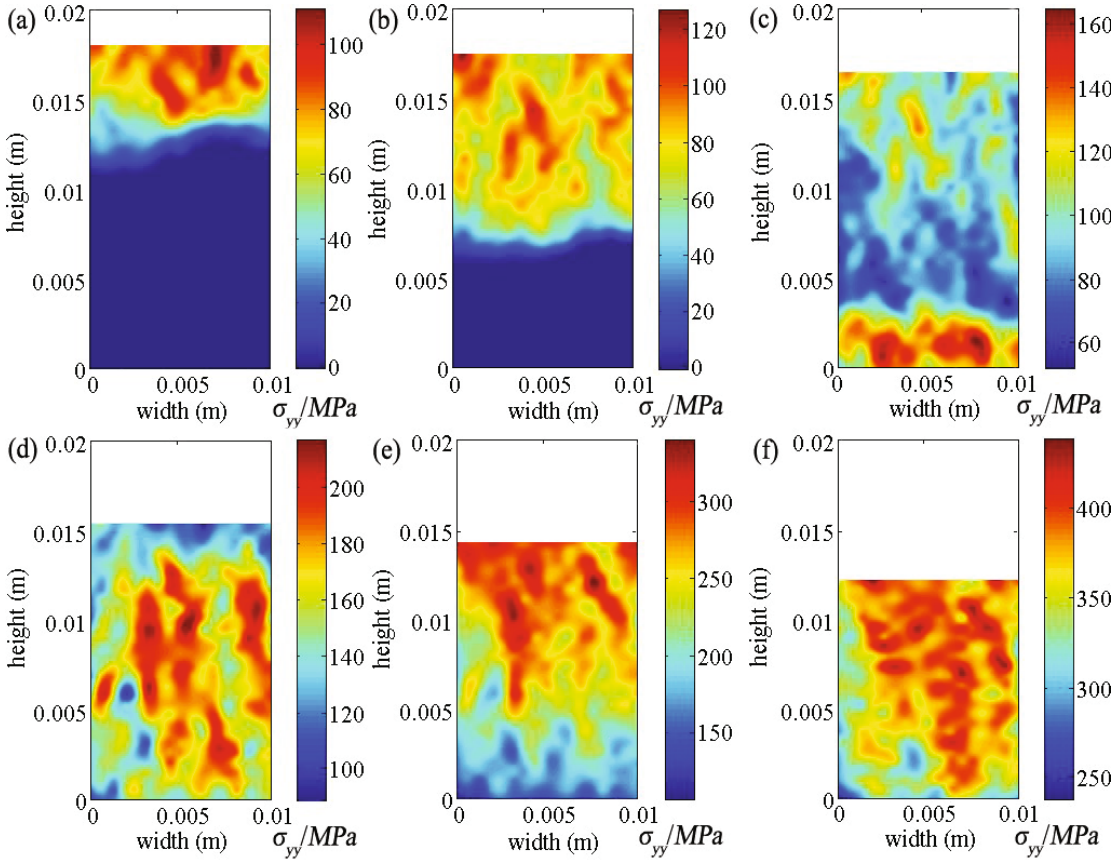

Fig. 5. (Color online) Distribution of stress at different moments (0.5, 0.8, 1.3, 1.7, 2.25, and 4 ms).

velocity and compare it to the sound velocity in the particles in the future. Furthermore, the stress distribution change is dynamic. The parts with stress concentration change from top to bottom, then reversely reflect, and become uniform in the end (Fig. 5). Interestingly, the distribution of stress shows the same changing trends as the structure of force chains.

The powder in HVC is condensed by an impact force. The evolution of force chains and the distribution of stress are related to the stress wave in HVC [4]; the same is not true for CC [30]. When the load attaches to the powder, the powder surface begins to move first. A collision occurs between the surface of the powder and the adjacent powder. Then, the adjacent powder begins to move. The disturbance is transferred layer by layer from top to bottom. Therefore, the force chains and the maximum stress distribution change from top to bottom. Meanwhile, the force chains and the maximum stress distribution can be reflected from the bottom. Finally, the force chains and stress become uniform. As a result, the distribution of stress shows an up-and-down moving trend. Changes in stress cause the evolution of force chains. When stress is concentrated in some parts, the force chains become dense. Meanwhile, a stable network of force chains promotes the distribution of stress change in the powder. The stress and the force chains interact and influence each other.

In order to investigate the differences in the force chains and the stress between HVC and CC, we carry out CC by using the same size model and powder parameters. The loading method is uniaxial compaction with a constant velocity of 2.2 mm/s, which is 1/1000 of the initial impact velocity in HVC. The CC stops when the final packing height is the same as that in the HVC. We use the normalized time to compare the evolution of force chains and stress (Fig. 6 and Fig. 7) because the entire simulation time of HVC is 4.59 ms while CC needs 3.26 s to achieve the same packing height as that in HVC.

The distributions of force chains and stress in CC are different from those in HVC. Although the value of the stress and the strength of force chains become higher with time in CC, the higher stress and the stronger force chains are always concentrated in the upper area of the powder. The area of stress concentration becomes larger as shown in Fig. 7(f) because it forms relative denser powder packing. The force chains and the stress in CC also do not show an up-and-down moving trend. The remarkable differences in the evolutions of the force chains and the stress can be attributed to the differences in the loading methods. The high-velocity impact load in HVC can cause powder to move sequentially and rapidly under an inertia effect while the constant low velocity load in

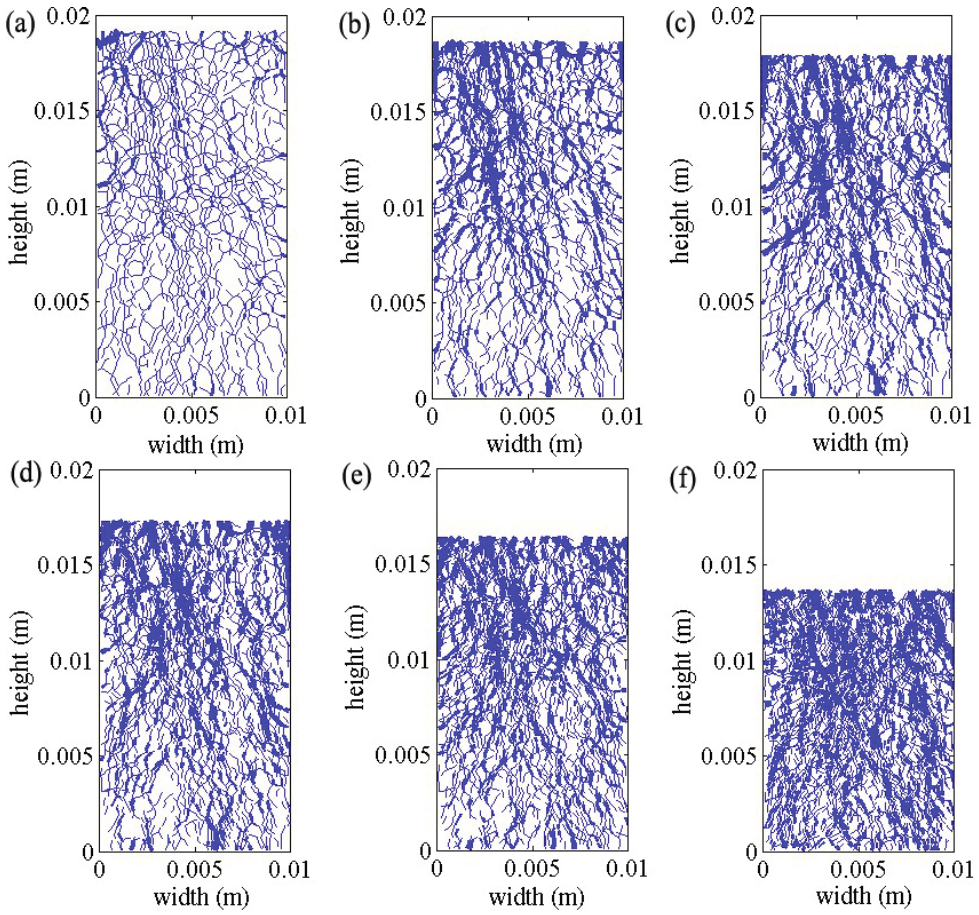

Fig. 6. (Color online) Structure of force chains at equivalent moments (0.35, 0.57, 0.92, 1.2, 1.6, and 2.84 s).

CC can cause powder to change its arrangement slowly. Thus, the force chains and the stress in HVC are different from those in CC.

2. Relation between force chain length and change of stress

The force chain length can be influenced by the structure and the evolution of the powder. Note that stress in HVC has a considerable influence on the motion of the powder. Hence, stress can cause changes to the force chain length to a certain extent. To quantitatively capture the relation between force chain length and stress, we analyze the normalized length of the force chains and the stress (Fig. 8). The correlation coefficient between the force chain length and the stress is -0.8559. Force chain lengths decrease as stress increases gradually. The high stress in HVC can cause the force chains to break and reorganize into shorter ones. The proportion of the different force chain lengths, which means the number ratio of different length force chains to all force chains, can explain this finding to some extent.

The PDFs of the force chain length show an exponentially decreasing trend, as shown in Fig. 9(a). Note that force chains with lengths longer than $15<d>$ can not be considered because they only occupy a small proportion of all force chains. Iikawa *et al.* [31] reported that the PDFs of force chain length can be fitted by using a linear function under manual tapping. Although manual tapping is also an instantaneous loading process, the strength of the load in HVC is dissimilar; thus, the evolution of different force chain lengths varies. The PDFs of force chain length can be fitted as $P(l) = Ae^{-Bl}$. With HVC, the parameters A and B of the exponential function increase gradually. This trend means that the proportion of short force chains grows steadily. The proportion of force chains with three particles differ at 0.5, 0.8, and 1.3 ms, but they are almost the same at 1.3, 1.7, 2.25 and 4 ms. The proportion of force chains with three particles is greater than the others and increases constantly. The comparison of Figs. 4 and 9 indicates that the force chains spread over all the powder with the proportion of force chains with three particles increasing sharply. As mentioned, the proportion of force chains with three particles rises quickly when the force chains and the stress begin to spread to all the powder. Moreover, the change in the proportion of force chains with

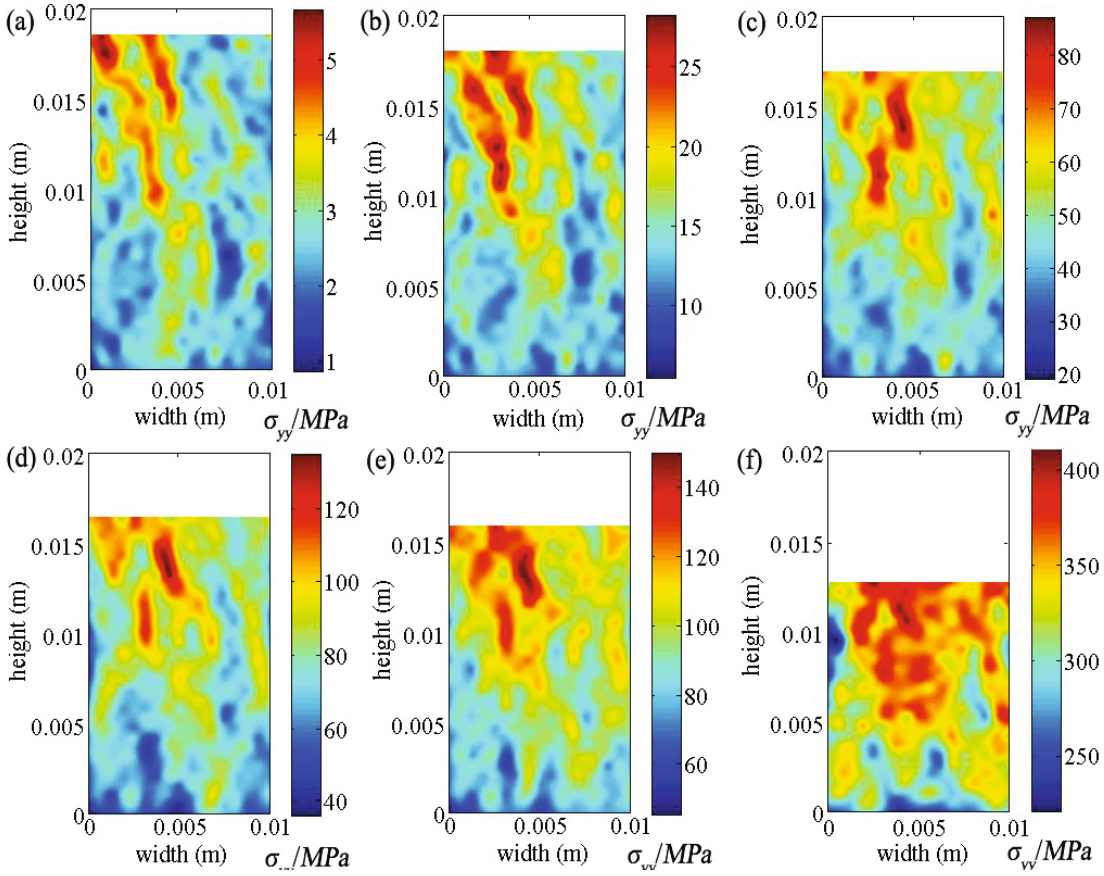

Fig. 7. (Color online) Distribution of stress at equivalent moments (0.35, 0.57, 0.92, 1.2, 1.6, and 2.84 s).

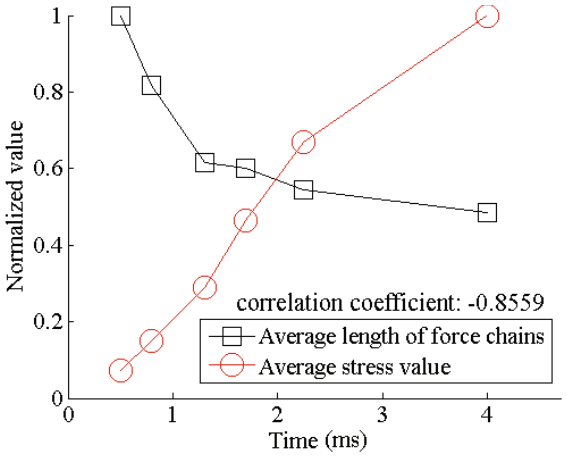

Fig. 8. (Color online) Comparison of normalized average values of the stress and the force chain length at 0.5, 0.8, 1.3, 1.7, 2.25, and 4 ms.

three particles is small when the force chains and the stress fill all the powder. A high-velocity impact load can cause the force chains and the stress to fill all the powder gradually according to Figs. 4 and 5. It can also promote the evolution of the distribution of force chain lengths, as shown in Fig. 9. The variations in force chain lengths with time are shown in Fig. 9(b). The proportion of force chains with lengths that are shorter than 4<d> (include 3<d> and 4<d>) increases gradually. Conversely, the proportion of force chains with lengths that are longer than 8<d> decreases gradually. Meanwhile, the proportion of force chains with lengths that are shorter than 8<d> and longer than 4<d> (include 5<d>, 6<d>, 7<d> and 8<d>) keeps fluctuating. This outcome suggests that long force chains may break under stress and become shorter force chains in HVC. From Fig. 5, the change in force chain lengths is obvious during stress transmission from top to bottom, but it is not obvious when stress transmits from bottom to top or stress is uniformly distributed.

3. Relation between force chain strength and stress magnitude

The above analysis of force chain lengths in HVC can represent the length geometric structure of force chains. The substantial impact load in HVC may cause the contact force to change rapidly. Hence, force chain strength and stress magnitude may change significantly. Many researchers [32, 33] emphasize the value of force chains

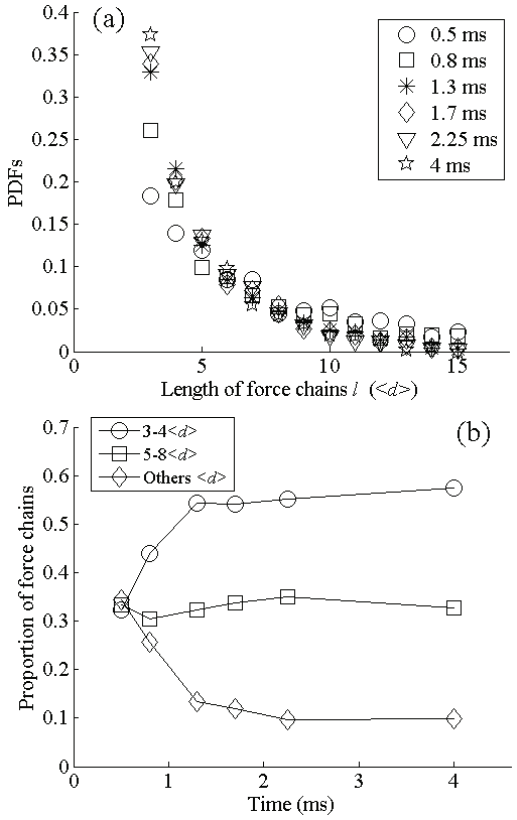

Fig. 9. (a) PDFs of force chain length at different moments (0.5, 0.8, 1.3, 1.7, 2.25, and 4 ms). (b) Variations in the force chain lengths with time.

and ignore their relation to geometric structure. Force chain strength can show the relation between force and length. It can represent the loading condition of force chains accurately.

We the introduce force chain strength p_i to describe the load bearing capacity of force chains. It is defined as

$$p_i = \frac{\sum_{k=1}^{S} f_k}{l_{\mathrm{i}}}, \tag{11}$$

where f_k is the contact force of the k-th contact, l_i is the length of the i-th force chains, S is the number of contacts of the i-th force chain, and the value of S is equal to Ni-1, with Ni being the number of particles of the i-th force chain. High strength shows that the contact force is concentrated on this force chain. The distribution of force chain strengths changes from top to bottom, reflects back, and ultimately becomes uniform (Fig. 10). Force chains are strong at bright parts. At 0.5 and 0.8 ms, strong force chains are located in the upper area of the powder. While at 1.3 ms they are concentrated in the lower area of the powder. With HVC, the distribution of force chain strengths is spread throughout the whole powder. Strong force chains are concentrated in most areas of the powder at 1.7 ms and in the upper parts at 2.25 ms. Finally, the distribution of force chain strengths represents a disordered state. Compared with the distribution of stress in Fig. 5, parts with strong force chains are due to stress concentration. Force chains can become strong such that the stress can transfer through them. Compared with the structure of force chains in Fig. 4, dense force chains may have great strength. Dense force chains have complex crossings with one another and stable structures, making them strong. Force chains and stress are interrelated in HVC. When impact loads are applied on the surface of the powder, the force chains organize and spread gradually, and the stress is transferred through the force chains. Thus, parts with strong force chains change with the evolution of the stress concentration.

To quantitatively determine the relation between force chain strength and stress, we analyze the averaged and the normalized strength of force chains and value of stress in the entire sample (Fig. 11). Force chain strength increases slowly, then sharply, and finally slowly. With HVC, the force chains spread over all the powder gradually such that force chain strengths increase slowly. When the force chains begin their growth in the whole system, their strength increases sharply. Force chain strength increases slowly at the end of HVC due to the low velocity load. The average stress value in the entire sample has the same changing trend as the strength of force chains. Their correlation coefficient exceeds 0.9773. This outcome confirms that they are interrelated and closely related.

4. Relation between the variations in the collimation coefficient and the stress

The straightness of force chains plays an important role in supporting the great external load in HVC. It represents the capability to resist the buckling of force chains. The force chains in HVC can experience quicker buckling, collapse, and reorganization than those in CC. Thus, investigating the relation between stress and straightness of the force chains is necessary.

We introduce the collimation coefficient of force chains δ_i to judge whether the force chains represent a linear chain structure. This coefficient is defined as

$$\delta_i = 1 - \frac{\sum_{p=1}^{M} \theta_p}{180^\circ \times M}, \tag{12}$$

where θ_p is the included sharp angle between p-th adjacent contact pairs of the i-th force chain, M is the number of adjacent contact pairs of the i-th force chain, and the value of M is equal to Ni-2. The value of δ_i is limited to [0, 1]. A small collimation coefficient means a large probability of buckling and collapse.

Overall, the collimation coefficient increases gradually as shown in Fig. 12(a). Specifically, the slope of the

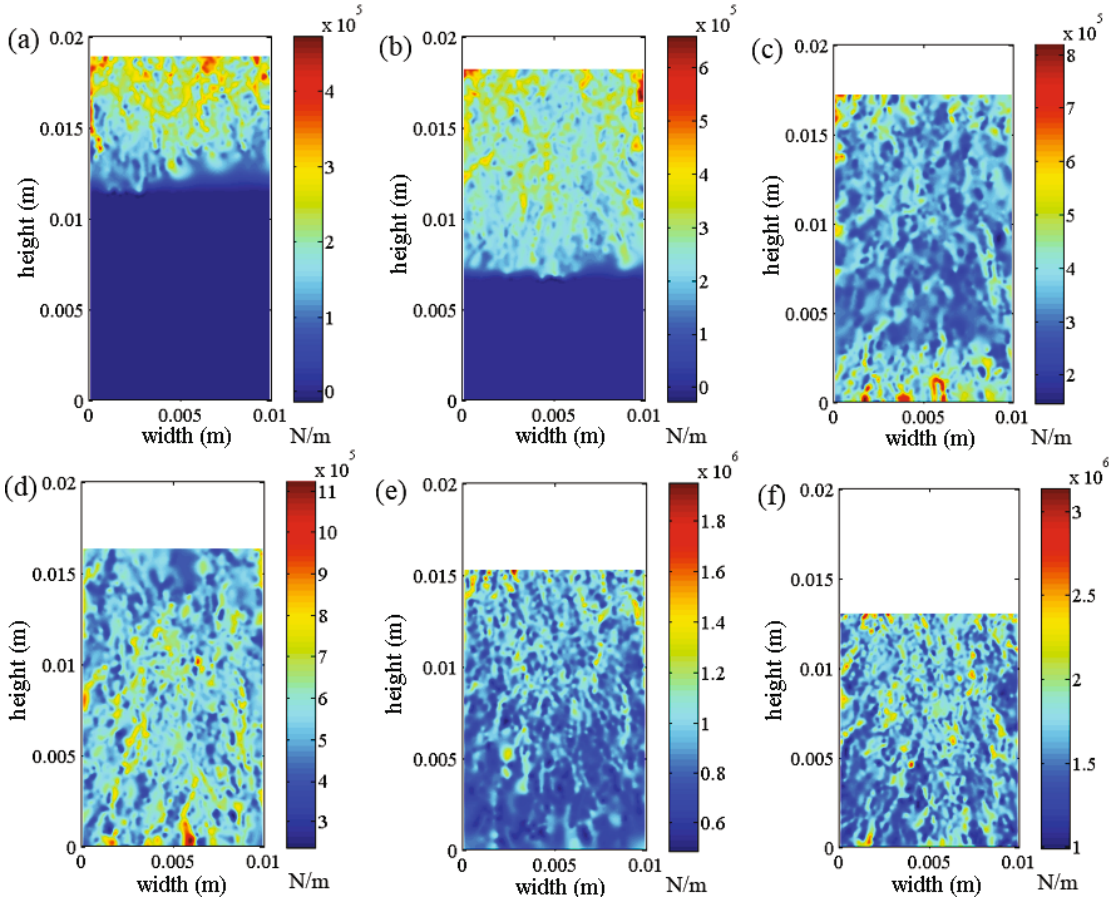

Fig. 10. (Color online) Distribution of force chain strengths at different moments (0.5, 0.8, 1.3, 1.7, 2.25, and 4 ms).

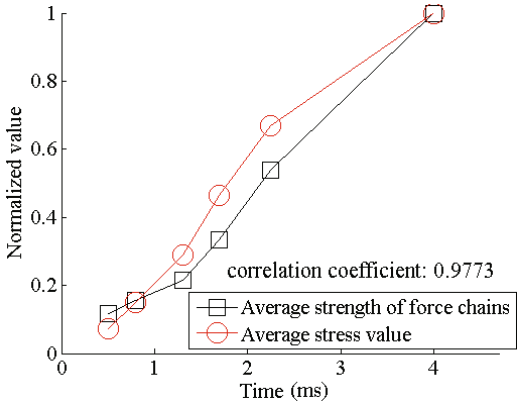

Fig. 11. (Color online) Comparison of the normalized values of the stress and the strength of force chains at 0.5, 0.8, 1.3, 1.7, 2.25, and 4 ms.

increase is high from 0.5 ms to 2.25 ms. By contrast, the slope of increase is low from 2.25 ms to 4 ms. The difference in slope increase is attributed to the characteristics of HVC. An instantaneous impact load can cause the stress to transmit upward and downward alternately (Fig. 5). When stress transmits from the top to the bottom of the powder and transmits reversely from 0.5 ms to 2.25 ms, the average collimation coefficient has high increased slope because force chains should form a stable supporting structure and the organizational process of force chains is rapid. When the stress becomes uniform in the powder from 2.25 ms to 4 ms, the average collimation coefficient has a small increasing slope because the structure of the powder does not change as much as before.

Compared with the value of stress in Fig. 5, the straightness of force chains improves with increasing stress during HVC. This finding means that stress may cause force chains to have good straightness. The ratio of long force chains (longer than $6<d>$) decreases, but the ratio of short force chains (shorter than $6<d>$) increases, as shown in Fig. 12(b). Short force chains have better straightness in general, as shown in Fig. 12(c), because the short force chains can be more easily made straight under stress. Besides, the long force chains have better straightness at about 1.3 ms because the stress transmits from bottom to top and may readily cause long force chains to improve their straightness. When the stress gradually becomes uniform in the system, the short force chains will have better straightness again.

5. Relation between the directional coefficient of the force chains and the direction of the principal stress

The above analysis focuses on the value of the stress and its relation to the quantitative characteristics of force chains. Stress has direction and may also cause force chains to change their directions. The principal stress angle is calculated as follows [34]:

$$\varphi_{\max} = \frac{1}{2}\arctan\left(\frac{\sigma_{xy}}{\sigma_{xx} - \sigma_{yy}}\right), \tag{13}$$

where σ_{xy}, σ_{xx} and σ_{yy} are the average shear stress, X-stress, and Y-stress, respectively. The principal stress angle changes from isotropic and irregular (0.5 and 0.8 ms) to anisotropic (1.3, 1.7, 2.25, and 4 ms) gradually, as shown in Fig. 13. The direction of maximum principal stress is expressed by the long axis with cross symbols, and the direction of minimum principal stress is expressed by the short axis with cross symbols. This outcome indicates that the direction of stress tends to change to the direction of the impact load in HVC. The impact load can generate pressure along the y-direction, and the powder begins to move and rearrange such that the stress shows anisotropy. Moreover, the direction of the principal stress angle near the wall tilts to the central axis of the powder. This phenomenon may be attributed to the friction characteristics of compacting powder [35]. The powder near the wall may be influenced by friction and exhibit low probability to flow. By contrast, the inside powder has high probability to flow. Hence, the principal stress angle shows tilting near the wall.

We introduce a directional coefficient σ to describe the orientation of force chains. The directional coefficient shows the whole directionality and the extended direction of force chains. Each force chain is composed of many segments, where the k-th segment has length d_k and angle θ_k relative to the direction of gravity. This coefficient is defined as [36]

$$\sigma_i = \left(\frac{2}{l_i}\sum_{k=1}^{S} d_k \cos^2\theta_{\mathrm{k}}\right) - 1. \tag{14}$$

The value of σ_i is limited to $[-1, 1]$. If σ_i is closer to ± 1, then the force chain shows great anisotropy.

Figure 14 shows the distribution of the directional coefficients at different moments. The red part shows the force chains that spread toward the direction parallel to gravity. Meanwhile, the blue part indicates force chains that spread toward the direction vertical to gravity. The color bar in Fig. 14 is not limited in $[-1, 1]$ because of the interpolation method of the cloud map. Force chains parallel to the direction of gravity are concentrated along the border at 0.5 and 0.8 ms according to Fig. 4. Force chains that are parallel to the direction of gravity are spread over all the powder, but they are more concentrated in the middle-lower areas of the powder at 1.3 ms.

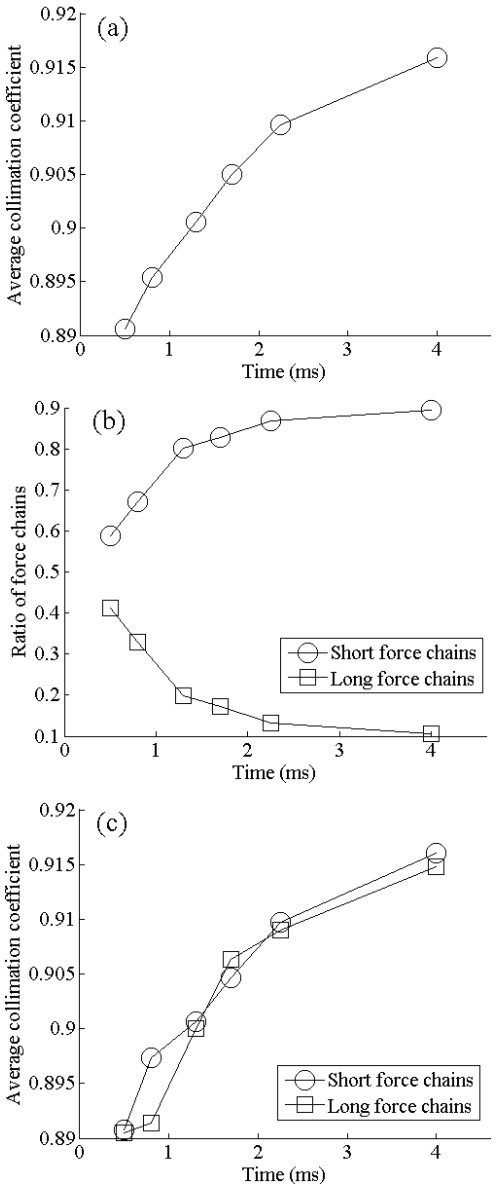

Fig. 12. (a) Variation of the collimation coefficient at different moments (0.5, 0.8, 1.3, 1.7, 2.25, and 4 ms). (b) Ratio of long and short force chains. (c)Collimation coefficients of long and short force chains. Fig. 13. Distribution of principal stress angle at different moments (0.5, 0.8, 1.3, 1.7, 2.25, and 4 ms).

The force chains that are parallel to the direction of gravity are more concentrated in the upper and the lower areas of the system at 1.7 ms. Furthermore, the force chains that are parallel to the direction of gravity are concentrated in the middle-lower areas of the powder at 2.25 ms. Finally, the distribution of the directional coefficient becomes uniform again at 4 ms. Other reports [16, 26] demonstrate the anisotropy of force chains in granular matter. However, the quantitative analysis of the directional distribution can present the direction of force chains directly.

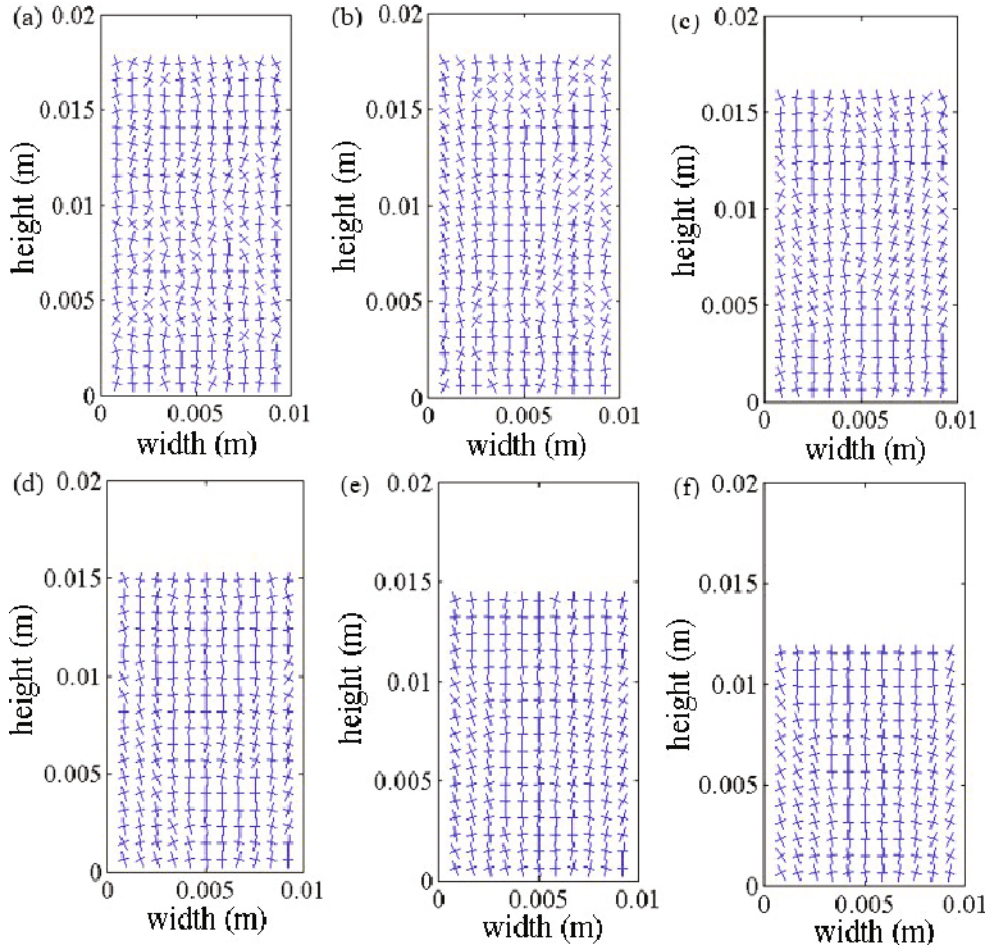

Fig. 13. (Color online) Distribution of principal stress angle at different moments (0.5, 0.8, 1.3, 1.7, 2.25, and 4 ms).

Compared with the distribution of stress in Fig. 5, that in Fig. 14 illustrates that stress can promote the spread of force chains toward the direction of the external impact load in HVC. The parts in which force chains are parallel to the direction of gravity (red parts) do not encounter the phenomenon of stress concentration. In parts with stress concentration, the stress may cause the force chains to change their direction across one another, making the absolute direction coefficient relatively low in general. Specifically, parts in which force chains are parallel to the direction of gravity have phenomenon of stress concentration at 1.3 ms because the substantial difference in stress in the lower and the middle areas of the powder can cause the force chains to spread in the direction of gravity.

Compared with the change in the principal stress angle shown in Fig. 13, the principal stress angle is almost isotropic at 0.5 and 0.8 ms, and only small parts have force chains that are parallel to the direction of gravity. Furthermore, the principal stress angle is anisotropic and is inclined to the direction of gravity at 1.3, 1.7, 2.25, and 4 ms, and most parts have force chains that are parallel to the direction of gravity. The direction of force chains and the principal stress angle may exhibit the same change from isotropy to anisotropy because the great impact energy of HVC can promote alternations of the direction of stress and force chains in the powder.

Establishing the quantitative relation between the principal stress angle and the directional coefficient is necessary. The principal stress angle coefficient of the i-th force chain is calculated as $\xi_i = \frac{|\beta_{\max}|}{90^\circ}$. A small ξ_i means that the principal stress angle is close to the y-direction. The principal stress angle coefficient decreases initially and then remains stable, as shown in Fig. 15. By contrast, the averaged and the normalized directional coefficients of force chains increase initially and then remain stable. A negative correlation exists between them, and the correlation coefficient is -0.9317. Such an outcome means that they have good correlation and are interrelated. The principal stress angle coefficient suggests that the stress changes from isotropy to anisotropy under an impact load. The directional coefficient reveals that the force chains change from isotropy to anisotropy as well.

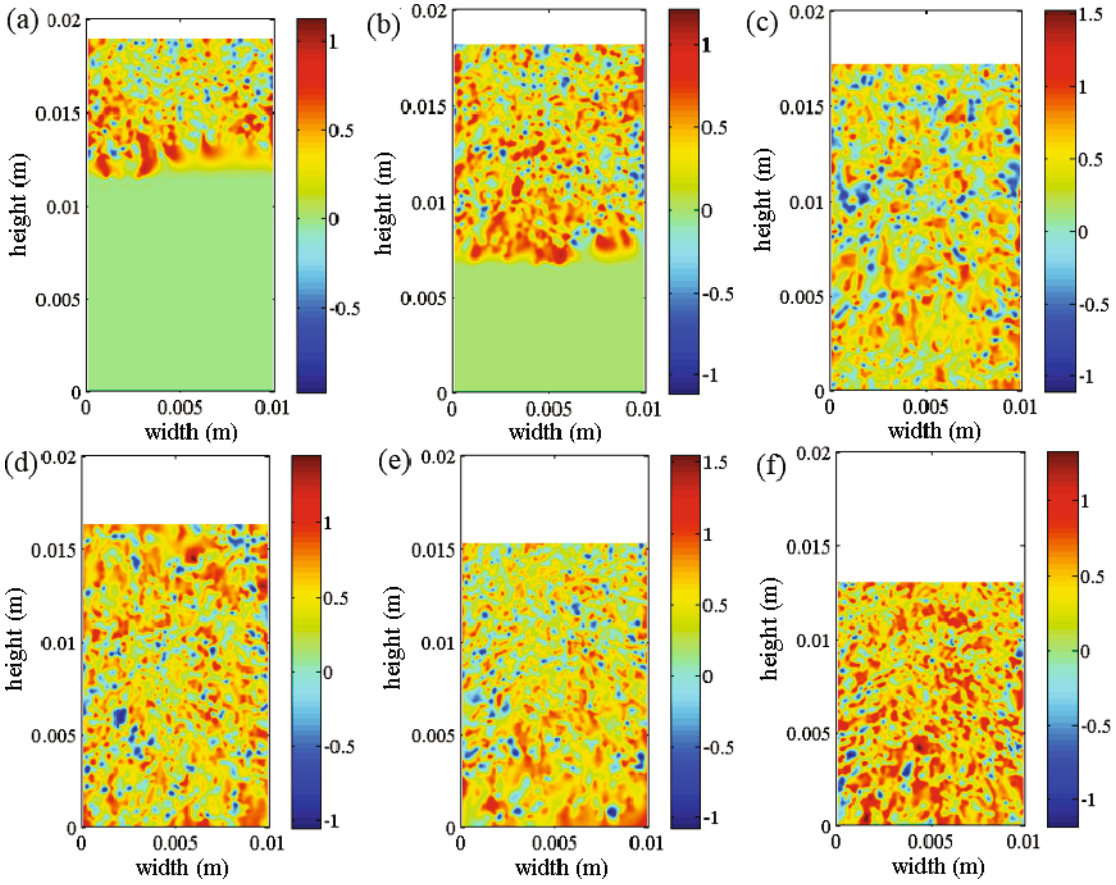

Fig. 14. (Color online) Spatial distribution of the directional coefficient of force chains at different moments (0.5, 0.8, 1.3, 1.7, 2.25, and 4 ms).

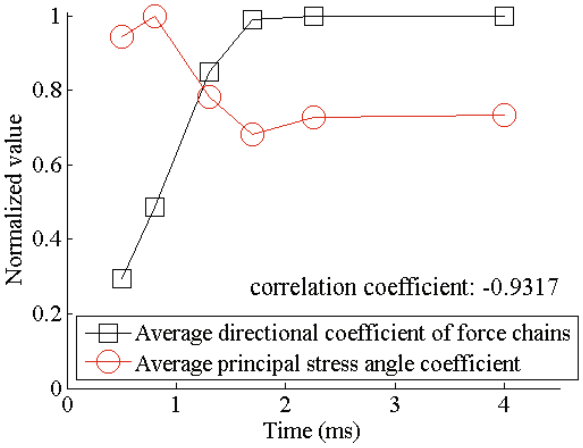

Fig. 15. (Color online) Comparison of normalized values of the principal stress angles and the directional coefficients of force chains at 0.5, 0.8, 1.3, 1.7, 2.25, and 4 ms.

IV. CONCLUSION

In this study, HVC was simulated by using the DEM, and the stress and force chains were investigated. Furthermore, the relation between the stress and force chains was examined. The following main conclusions were drawn:

(1) The stress and force chains in HVC evolve from top to bottom and then reflect backwards. Parts with stress concentration correspond to locations that have dense force chains with great contact force. However, the higher stress or stronger force chains are always concentrated in the upper areas of the powder in CC and do not show an up-and-down moving trend.

(2) An increase in the stress can cause the length of force chains to become shorter. Such a relation may be explained by the fact that when the proportion of long force chains decreases, the newly organized force chains may be shorter. The short force chains may generally have better straightness under stress.

(3) Parts with force chains with high strength have a corresponding stress concentration. The increase in the average collimation coefficient of the force chains also shows good agreement with the transition of the stress. Force chains parallel to the direction of gravity are concentrated in parts that lack stress concentration. Furthermore, the normalized average principal stress angle and directional coefficient of force chains show a good

correlation. The force chains and the stress all change from isotropy to anisotropy.

We find some interesting conclusions about force chains, stress and their relations in HVC. Experiments on capturing the force chains and the stress of the powder directly will be carried out in the next research. In order to verify the results in this paper, we are considering that use a transparent powder and a photoelasticity method in the next research.

ACKNOWLEDGMENTS

The authors wish to thank the National Natural Science Foundation of China for its financial support under Grant No. 51475135 and Grant No. 11472096.

REFERENCES

[1] J. Z. Wang, X. H. Qu, H. Q. Yin, M. J. Yi and X. J. Yuan, Powder Technol. **192**, 131 (2009).
[2] D. F. Khan *et al.*, Mater. Design **50**, 479 (2013).
[3] H. Li *et al.*, Mater. Design **57**, 546 (2014).
[4] Z. Q. Yan, F. Chen and Y. X. Cai, Powder Technol. **208**, 596 (2011).
[5] D. F. Khan *et al.*, Mater. Design **54**, 149 (2014).
[6] A. R. Khoei, S. O. R. Biabanaki and S. M. Parvaneh, Appl. Math. Model **37**, 443 (2013).
[7] M. C. Zhou *et al.*, Powder Technol. **305**, 183 (2017).
[8] P. Han *et al.*, Powder Technol. **314**, 69 (2017).
[9] F. Huang, X. Z. An, Y. X. Zhang and A. B. Yu, Powder Technol. **314**, 39 (2017).
[10] M. Shoaib, L. Kari and B. Azhdar, Powder Technol. **217**, 394 (2012).
[11] S. Wang and Z. S. Zheng, Particuology **31**, 49 (2017).
[12] M. J. Yi, H. Q. Yin, J. Z. Wang, X. J. Yuan and X. H. Qu, Front. Mater. Sci. China **3**, 447 (2009).
[13] J. P. Bayle and F. Jorion, Proc. Chem. **7**, 431 (2012).
[14] C. Giusti, L. Papadopoulos, E. T. Owens, K. E. Daniels and D. S. Bassett, Phys. Rev. E **94**, 032909 (2016).
[15] Y. M. Huang and K. E. Daniels, Granular Matter **18**, 85 (2016).
[16] A. Tordesillas, E. H. James and T. T. Steven, Phys. Rev. E **89**, 042207 (2014).
[17] A. Tordesillas, J. Y. Shi and T. Timothy, Anal. Met. **35**, 264 (2011).
[18] A. Tordesillas, Phil. Mag. **32**, 4987 (2007).
[19] O. Masanobu and I. Kazuyoshi, Int. J. Eng. Sci. **38**, 1713 (2000).
[20] P. A. Cundall, Minnesota: Itasca Consulting Group Inc. (2004).
[21] S. Wang, Z. S. Zhen and W. Zhou, Acta Phys. Sin. **60**, 128101 (2011).
[22] H. Kim, M. P. Wagoner and W. G. Buttlar, J. Mater. Civil. Eng. **20**, 552 (2008).
[23] Y. He *et al.*, J. Mater. Process. Tech **249**, 291 (2017).
[24] C. L. Martin, D. Bouvard and S. Shima, J. Mech. Phys. Solids **51**, 667 (2003).
[25] A. H. Kharaz and D. A. Gorham, Phil. Mag. Lett. **80**, 549 (2000).
[26] H. Teufelsbauer, Y. Wang, M-C. Chiou and W. Wu, Granular Matter **11**, 209 (2009).
[27] J. F. Peters, M. Muthuswamy, J. Wibowo and A. Tordesillas, Phys. Rev. E **72**, 041307 (2005).
[28] Q. C. Sun, F. Jin and J. G. Liu, Int. J. Mod. Phys. B **24**, 5743 (2010).
[29] W. Zhang, J. Zhou, S. W. Yu, X. J. Zhang and K. Liu, Chin. J. Appl. Mech. **35**, 155 (2018).
[30] H. Z. Zhang *et al.*, Powder Technol. **288**, 435 (2016).
[31] N. Iikawa, M. M. Bandi and H. Katsuragi, J. Phys. Soc. Jpn. **84**, 094401 (2014).
[32] F. J. Meng, K. Liu and W. Wang, Tribol. Trans. **58**, 70 (2015).
[33] R. C. Hurley, S. A. Hall, J. E. Andrade and J. Wright, Phys. Rev. Lett. **117**, 098005 (2016).
[34] H. J. Lai, J. J. Zheng, J. Zhang, R. J. Zhang and L. Cui, Comput. Geotech. **61**, 13 (2014).
[35] C. Y. Wu *et al.*, Powder Technol. **152**, 107 (2005).
[36] N. Iikawa, M. M. Bandi and H. Katsuragi, Phys. Rev. E **94**, 032909 (2016).